THE JOURNAL OF BIOLOGICAL CHEMISTRY
Vol. 278, No. 19, Issue of May 9, pp. 17075–17083, 2003
Printed in U.S.A.


# Farnesyl Pyrophosphate Synthase Is an Essential Enzyme in *Trypanosoma brucei*

*IN VITRO* RNA INTERFERENCE AND *IN VIVO* INHIBITION STUDIES*

Received for publication, October 11, 2002, and in revised form, February 19, 2003
Published, JBC Papers in Press, March 4, 2003, DOI 10.1074/jbc.M210467200

**Andrea Montalvetti‡, Alexis Fernandez‡, John M. Sanders§, Subhash Ghosh§, Erin Van Brussel§, Eric Oldfield§, and Roberto Docampo‡¶**

*From the ‡Laboratory of Molecular Parasitology, Department of Pathobiology and Center for Zoonoses Research, University of Illinois at Urbana-Champaign, Urbana, Illinois 61802 and the §Department of Chemistry, University of Illinois at Urbana-Champaign, Urbana, Illinois 61801*

**We report the cloning and sequencing of a gene encoding the farnesyl pyrophosphate synthase (FPPS) of *Trypanosoma brucei*. The protein (TbFPPS) is an attractive target for drug development because the growth of *T. brucei* has been shown to be inhibited by analogs of its substrates, the nitrogen containing bisphosphonates currently in use in bone resorption therapy. The protein predicted from the nucleotide sequence of the gene has 367 amino acids and a molecular mass of 42 kDa. Several sequence motifs found in other FPPSs are present in TbFPPS, including an 11-mer peptide insertion present also in the *Trypanosoma cruzi* FPPS. Heterologous expression of *TbFPPS* in *Escherichia coli* produced a functional enzyme that was inhibited by several nitrogen-containing bisphosphonates, such as pamidronate and risedronate. Risedronate was active *in vivo* against *T. brucei* infection in mice (giving a 60% survival rate), but pamidronate was not effective. The essential nature of *TbFPPS* was studied using RNA interference (RNAi) to inhibit the expression of the gene. Expression of *TbFPPS* double-stranded RNA in procyclic trypomastigotes caused specific degradation of mRNA. After 4 days of RNAi, the parasite growth rate declined and the cells subsequently died. Similar results were obtained with bloodstream form trypomastigotes, except that the RNAi system in this case was leaky and mRNA levels and parasites recovered with time. Molecular modeling and structure-activity investigations of enzyme and *in vitro* growth inhibition data resulted in similar pharmacophores, further validating TbFPPS as the target for bisphosphonates. These results establish that FPPS is essential for parasite viability and validate this enzyme as a target for drug development.**

The *Trypanosoma brucei* group of parasites causes African trypanosomiasis (sleeping sickness) in humans, and nagana in animals and is responsible for heavy socioeconomic losses in most countries of sub-Saharan Africa (1). Therapy against African sleeping sickness is unsatisfactory because of the toxicity of currently available drugs, together with the development of drug resistance (2).

A number of bisphosphonates have recently been shown to have significant activity against the proliferation of *T. brucei* and other parasites *in vitro* (3, 4) and also have curative effects in *in vivo* models of visceral (5) and cutaneous (6) leishmaniasis. Bisphosphonates are pyrophosphate analogs in which the oxygen bridge between the two phosphorus atoms has been replaced by a carbon substituted with various side chains. Several bisphosphonates are potent inhibitors of bone resorption and are in clinical use for the treatment and prevention of osteoporosis, Paget's disease, hypercalcemia caused by malignancy, and tumor metastases in bone (7–10). Many bisphosphonates, such as pamidronate, alendronate, and risedronate, are known to inhibit farnesyl pyrophosphate synthase (FPPS)[1] (11–16), and in so doing, they inhibit the formation of farnesyl pyrophosphate, a compound used in protein prenylation and in the synthesis of dolichols, ubiquinones, heme *a*, and sterols. Although a recombinant FPPS from *Trypanosoma cruzi* has recently been shown to be potently inhibited by bisphosphonates (17), the question as to whether or not this enzyme is essential for trypanosomatid viability has remained unresolved. Here, we report the results of RNA interference (RNAi) studies together with *in vitro* and *in vivo* inhibition studies that demonstrate that FPPS is indeed an essential cellular component in *T. brucei*.

## EXPERIMENTAL PROCEDURES

*Materials*—Fetal bovine serum, Dulbecco's phosphate-buffered saline, protease inhibitor mixture, geranyl pyrophosphate (GPP), and isopentenyl pyrophosphate (IPP) were purchased from Sigma. Fetal bovine serum (normal and dialyzed) was from Atlanta Biologicals (Norcross, GA) and Serum Plus was from JRH Biosciences (Lenex, KS). Restriction enzymes, T4 DNA ligase, *Taq* polymerase, the Klenow fragment of DNA polymerase, Trizol reagent, and 0.24–9.5-kb RNA ladder were from Invitrogen. pCR2.1-TOPO cloning kit, and Superscript II RT were from Invitrogen. Hybond-N nylon membrane, PD-10 desalting column, and [$\alpha$-$^{32}$P]dCTP (3000 Ci/mmol) were obtained from Amersham Biosciences. [4-$^{14}$C]IPP (57.5 mCi/mmol) was from PerkinElmer Life Sciences. The pET-28a$^{+}$ expression system and Benzonase™ nu-

* This work was supported in part by grants from the World Health Organization Special Programme for Research and Training in Tropical Diseases (to R. D. and to E. O.), the American Heart Association, National Center (to R. D.), and United States Public Health Service National Institutes of Health Grant GM-65307 (to E. O. and R. D.). The sequencing work was supported by an award from the National Institute of Allergy and Infectious Diseases, National Institutes of Health. The costs of publication of this article were defrayed in part by the payment of page charges. This article must therefore be hereby marked "*advertisement*" in accordance with 18 U.S.C. Section 1734 solely to indicate this fact.

¶ To whom correspondence should be addressed: Laboratory of Molecular Parasitology, Dept. of Pathobiology and Center for Zoonoses Research, College of Veterinary Medicine, University of Illinois, 2001 S. Lincoln Av., Urbana, IL. Tel: 217-333-3845; Fax: 217-244-7421; E-mail: rodoc@uiuc.edu.

[1] The abbreviations used are: FPPS, farnesyl pyrophosphate synthase; FPP, farnesyl pyrophosphate; GPP, geranyl pyrophosphate; IPP, isopentenyl pyrophosphate; TbFPPS, *Trypanosoma brucei* farnesyl pyrophosphate synthase; FBS, fetal bovine serum; RT, reverse transcripase; RNAi, RNA interference; Mops, 4-morpholinepropanesulfonic acid.

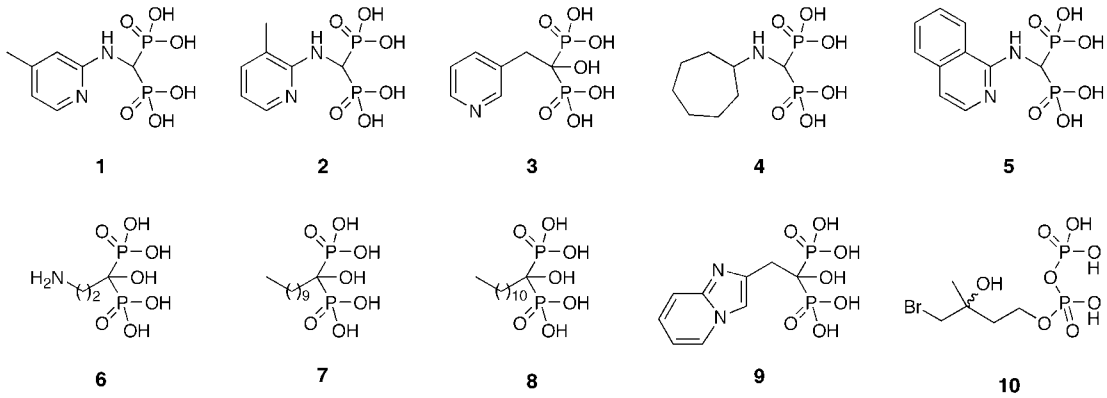


FIG. 1. **Structures of bisphosphonates (1–9) and the bromohydrin of IPP (phosphostim, 10).**

clease were from Novagen (Madison, WI). Nickel-nitrilotriacetic acid-agarose was obtained from Qiagen (Valencia, CA). *Pfu* DNA polymerase was from Stratagene (La Jolla, CA). The pZJM vector was a gift from Paul Englund (Johns Hopkins University, Baltimore, MD) (18). Oligonucleotides were synthesized at Integrated DNA Technologies, Inc. (Coralville, IA). All other reagents were analytical grade. Bisphosphonates and the bromohydrin pyrophosphate (Fig. 1) were synthesized using standard methods (3, 19, 20) and were characterized by C/H/N microanalysis and $^1$H NMR spectroscopy.

*Culture Methods*—Procyclic forms of *T. brucei,* strain ILTar 1, were grown in SDM-79 supplemented with 10% fetal bovine serum (FBS). Procyclic form cell line 29-13 and bloodstream form (cell line BF, with a single marker) co-expressing T7 RNA polymerase and Tet repressor were gifts from G. A. M. Cross (Rockefeller University) (21). Procyclic forms were grown in SDM-79 supplemented with 15% FBS or dialyzed FBS in the presence of G418 (15 $\mu$g/ml) and hygromycin (50 $\mu$g/ml). Bloodstream forms were grown in HMI-9 medium (22) supplemented with 10% FBS or dialyzed FBS with 10% Serum Plus, and G418 (2.5 $\mu$g/ml). Cell densities were determined using a Neubauer chamber. Procyclic forms were diluted to $1 \times 10^6$ cell/ml and bloodstream forms to $0.5 \times 10^5$ cell/ml and cultured in appropriate media. Growth curves were plotted by using the product of the cell density and the dilution factor.

*Cloning of the T. brucei FPPS Gene and DNA Sequencing*—A fragment of 428 bp of the *TbFPPS* gene was amplified using the oligonucleotide primers *TbFPPS1* (5′-GGCTATTTGTTAGTGAGGCT-3′) and *TbFPPS2* (5′-CTTCTGGCGCTTGTAAGTCT-3′) derived from a *T. brucei* genomic survey sequence (GenBank™ accession number AQ651702) that showed pronounced similarity to FPPSs of other organisms. Based on this sequence, we designed specific primers to obtain the entire coding sequence using the 5′-rapid amplification of cDNA ends system, version 2.0 (Invitrogen). The primer *TbFPPS2* was used for cDNA synthesis and the primers *Tb-5′-SL* (5′-AACGCTATTATTAGAACAGTTTCTG-3′), complementary to the *T. brucei* 5′-spliced leader sequence, and *TbFPPS3* (5′-CCCACAGAGTTTCTACGCTG-3′), complementary to sequences just upstream of the primer *TbFPPS2*, were used to amplify the 5′ end of the *TbFPPS*. The PCR was performed with 35 cycles of 94 °C for 1 min, 50 °C for 1 min, and 72 °C for 2 min, using 2.5 units of *Pfu* DNA polymerase, and cDNA as template, 200 pmol of each of the two primers, 1× *Pfu* buffer, and 0.2 mM dNTPs in a total volume of 50 $\mu$l. For 3′-rapid amplification of cDNA ends, cDNA was synthesized using oligo(dT) primer, and primers *TbFPPS1* and oligo(dT) were used to amplify the 3′ end of the gene. Two oligonucleotide primers based on the 5′- and 3′-untranslated regions of the *TbFPPS* gene were then used to amplify the entire coding sequence, using *Pfu* DNA polymerase and *T. brucei* genomic DNA as a template. PCR products were cloned into the pCR2.1-TOPO and sequenced. The predicted amino acid sequence of TbFPPS was aligned with the sequences of other FPPSs by using the Biology Workbench 3.2 utility.[2] The sequences alignment and phylogenetic tree were done using CLUSTAL W (23) and PHYLIP phylogeny packages (version 3.5c) (24) following the method of Saitou and Nei (25).

*Plasmid Constructs, Transfections, and Induction of RNAi*—A fragment corresponding to the *FPPS* from *T. brucei* (nucleotides 130–810) was amplified using the 5′ primer (CCGCTCGAGTTGGGCGGCAAATACAAC) and the 3′ primer (CCCAAGCTTGACTTTTCCTAGCCGCTC) having flanking *Xho*I and *Hin*dIII sites, respectively. The resulting 680-bp fragment was cloned into the pCR2.1-TOPO, verified by sequencing, and ligated into the corresponding restriction sites of the pZJM vector (26). For stable transfection of the procyclic form (cell line 29-13) and the bloodstream form (cell line BF) via integration into a rDNA spacer region, the vector was linearized by *Not*I digestion. Transfectants were selected using phleomycin (2.5 $\mu$g/ml) (18, 26). The procyclic forms were cloned 1 day after transfection by limiting dilution while the bloodstream forms were cloned immediately after electroporation, by splitting cells into 24 wells of a microtiter plate. For induction of RNAi, cells were cultured in the presence of tetracycline (1 $\mu$g/ml).

*Southern and Northern Blot Analyses, and Reverse Transcriptase-PCR*—Total genomic DNA from procyclic *T. brucei* was isolated by phenol extraction (27), digested with different restriction enzymes, separated on a 1% agarose gel, and transferred to nylon membranes. The blot was probed with a [$\alpha$-$^{32}$P]dCTP-labeled *TbFPPS*. After hybridization, the blot was washed three times in 2× SSC, 0.1% SDS at 65 °C (SSC is 0.15 M NaCl, 0.015 M sodium citrate). For the Northern blot analysis, total RNA was isolated from procyclic and bloodstream forms using Trizol reagent. RNA samples were subjected to electrophoresis in 1% agarose gels containing 1× Mops buffer (20 mM Mops, 0.08 M sodium acetate, pH 7.0, 1 mM EDTA) and 6.29% (v/v) formaldehyde, after boiling for 10 min in 50% (v/v) formamide, 1× Mops buffer, and 5.9% (v/v) formaldehyde. The gels were transferred to a Hybond-N filter and hybridized with a probe containing the entire coding sequence of the *TbFPPS* gene obtained by PCR. All Southern and Northern blots were visualized by autoradiography. A fragment of the $\alpha$-tubulin gene was used as a control in Northern blots (26). Densitometric analyses of Northern blots were performed by using a Kodak Digital Science Image Station 440 CF. Comparison of levels of *TbFPPS* transcription between non-induced and induced cells was performed by taking as a reference the densitometric values obtained with the *TbFPPS* transcripts from non-induced parasites. To analyze the level of *TbFPPS* mRNA in cells grown in the presence or absence of tetracycline, total RNA was also isolated from equal cell numbers and used for reverse transcriptase (RT)-PCR analysis using SuperScript II RT and the same set of primers that were used to amplify the fragment (680 bp) that was cloned into the pZJM vector.

*Expression and Purification of TbFPPS from E. coli*—For expression in *E. coli*, the entire coding sequence of the *TbFPPS* gene was amplified by PCR. Oligonucleotide primers for amplification of the FPPS coding region, *ATG-TbFPPS* (5′-CTAGCTAGCATGCCAATGCAAATG-3′) and *TGA-TbFPPS* (5′-CCCAAGCTTCACTTCTGGCGCTTGTA-3′), were designed so that *Nhe*I and *Hin*dIII restriction sites were introduced at the 5′ and 3′ ends for convenient cloning in the expression vector pET-28a$^+$ to give pETbFPPS, which was cloned and propagated in *Escherichia coli* DH5$\alpha$. Double-stranded DNA sequencing was performed to confirm that the correct reading frame was used, with the polyhistidine tag placed in the N-terminal position. Subsequently, pETbFPPS was used to transform *E. coli* BL21(DE3). Bacterial clones were grown in LB medium containing 50 $\mu$g/ml kanamycin. When induction was performed, bacterial cells transformed with *pETbFPPS* were first grown to an $A_{600}$ of 0.6 at 37 °C and then 1 mM isopropyl-$\beta$-D-thiogalactoside was added. After 5 h of growth at 37 °C, cells were pelleted by centrifugation and resuspended in lysis buffer (5 mM imidazole, 300 mM NaCl, 250 mM sucrose, 50 mM Tris-HCl, pH 7.2), incubated with 10 mg/ml lysozyme for 15 min on ice, then sonicated. The lysate was incubated with Benzonase™ nuclease for 15 min on ice, then centrifuged at 16,000 × *g*

[2] Workbench.sdsc.edu.

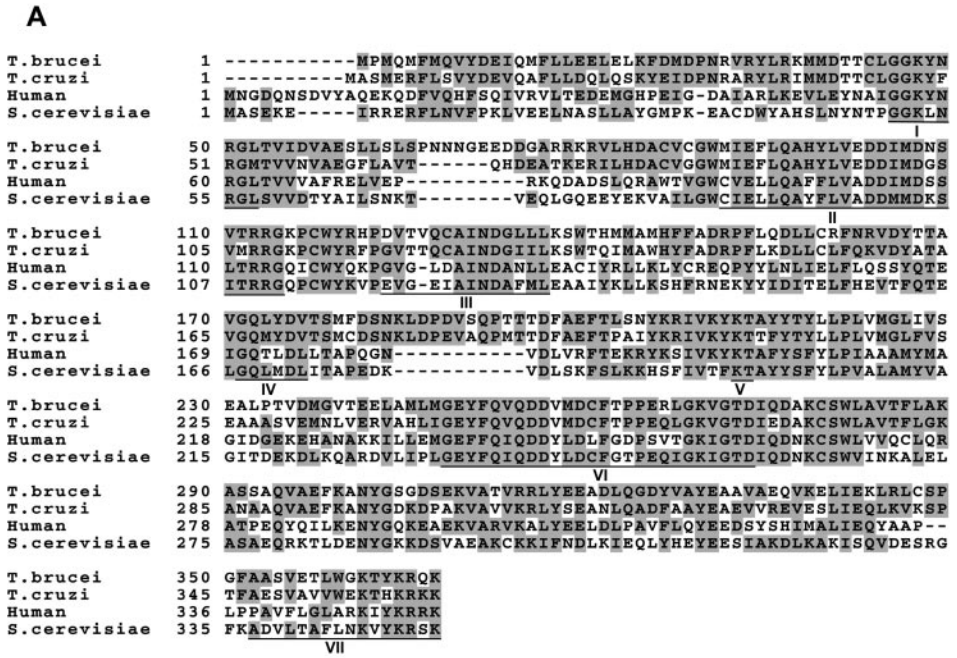


FIG. 2. **Sequence analysis of the FPPS from *T. brucei*.** *A*, comparison of the deduced amino acid sequence of *T. brucei* with other FPPSs. The deduced amino acid sequence of *T. brucei* FPPS (GenBank™ accession number AY158342) is compared with the sequences of *T. cruzi* (AF312690), human (P14324), and *S. cerevisiae* (J05091) synthases. Similar residues are *shaded*. The seven conserved regions I to VII are *underlined*. *B*, unrooted tree based upon FPPS amino acid sequences. The *bar* indicates a branch length corresponding to 0.2 substitutions per site. Distances were calculated using the Neighbor Joining (NJ) method of Saitou and Nei (25).

for 15 min. The supernatant was mixed with nickel-nitrilotriacetic acid-agarose for 1 h at 4 °C, then loaded onto a column and washed with lysis buffer in which the concentration of imidazole increased from 15 and 25 mM. Protein was eluted from the column with the same buffer but containing 500 mM imidazole. The eluted fraction was desalted with a PD-10 desalting column. Proteins were determined by the method of Bradford (28) with bovine serum albumin as a standard and analyzed for purity by SDS-polyacrylamide gel electrophoresis.

*Western Blotting and Generation of Antibodies against T. cruzi FPPS*—Total trypanosome proteins (30 $\mu$g of protein/lane) were subjected to SDS-polyacrylamide gel electrophoresis (10%). Electrophoresed proteins were transferred to nitrocellulose using a Bio-Rad Trans-blot apparatus. Membranes were probed with a 1:1,000 dilution of a rabbit anti-FPPS polyclonal antiserum prepared against recombinant *T. cruzi* FPPS (17). Bound antibodies were revealed by using goat anti-rabbit IgG (1:20,000) and the ECL™ chemiluminescent detection kit (Amersham Biosciences). To purify the *T. cruzi* FPPS antibodies, an affinity matrix was prepared by coupling 5 mg of *T. cruzi* FPPS to 1 ml of cyanogen bromide-activated Sepharose (Sigma). Immune serum (3 ml) was diluted 2-fold with phosphate-buffered saline and incubated with the affinity matrix overnight at 4 °C. Antibodies were eluted with 100 mM glycine, pH 2.5, and the eluate was neutralized with 0.1 volume of 2 M Tris-HCl, pH 8.0.

*FPPS Assay and Product Analysis*—The activity of the enzyme was determined by using the radiometric assay described previously (17). One unit of enzyme activity is defined as the activity required to incorporate 1 nmol of 4-[$^{14}$C]IPP into 4-[$^{14}$C]FPP in 1 min.

*Treatment of T. brucei-infected Mice*—BALB/c mice (8 weeks old) were infected intraperitoneally with 10,000 *T. brucei* bloodstream trypomastigotes (monomorphic strain 427 from clone MITat 1.4, otherwise known as variant 117). Starting the next day, mice were then treated intraperitoneally with pentamidine or bisphosphonates in 200 $\mu$l of

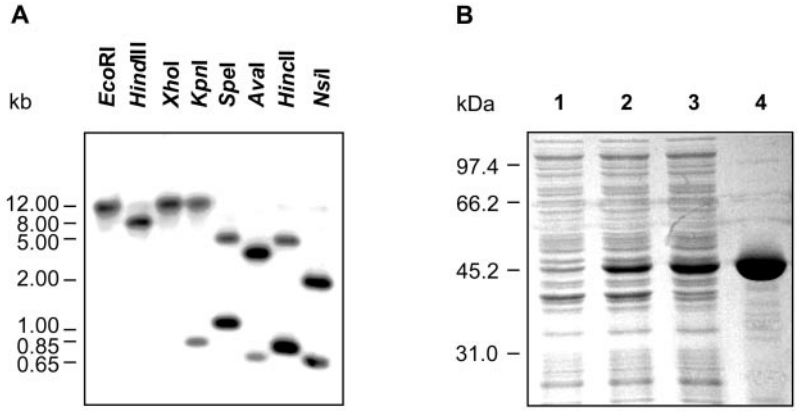


FIG. 3. **Southern blot analysis and purification of FPPS from *E. coli*.** *A*, total genomic DNA was digested with different endonucleases. The DNA fragments were separated in 1% (w/v) agarose, transferred to a nylon membrane, and hybridized with a $^{32}$P-labeled probe corresponding to the FPPS coding sequence. *B*, a SDS-polyacrylamide gel was stained with Coomassie Brilliant Blue. *Lane 1*, crude extract from pET-28a$^{+}$-transformed cell; *lane 2*, crude extract of *E. coli* BL21(DE3)/pETbFPPS; *lane 3*, soluble fraction from extract of *E. coli* BL21(DE3)/pETbFPPS; *lane 4*, nickel column purified fraction.

TABLE I
*Effect of divalent cations on FPPS from T. brucei*

FPPS activity was measured in the presence of the different concentrations of $MgCl_2$ or $MnCl_2$ as indicated, in a reaction medium containing 10 mM Hepes (pH 7.4), 2 mM dithiothreitol, 47 $\mu$M 4-[$^{14}$C]IPP (10 $\mu$Ci/$\mu$mol), 200 $\mu$M GPP, and 10 ng of recombinant protein (final volume 100 $\mu$l). Reactions were incubated for 30 min at 37 °C, stopped by the addition of HCl, and made alkaline with NaOH. The radioactive prenyl product was extracted with hexane. No activity was detected in the absence of $MgCl_2$ or $MnCl_2$ and presence of 10 mM EDTA. Values shown are mean ± S.D. of two experiments.

| Concentration | FPPS activity | |
|---|---|---|
| | $MgCl_2$ | $MnCl_2$ |
| *mM* | *units/mg* | |
| 0 | 1.6 ± 0.5 | 1.6 ± 0.5 |
| 0.5 | 660 ± 30 | 19 ± 2.5 |
| 1 | 740 ± 2 | 9.6 ± 0.1 |
| 5 | 840 ± 5 | 4.6 ± 2.2 |
| 10 | 840 ± 5 | 14 ± 0.6 |
| 20 | 670 ± 30 | 5.1 ± 2.4 |

0.9% sodium chloride solution for the times and doses indicated under "Results." Control mice received only the vehicle.

*Molecular Modeling*—Using an avian FPPS x-ray structure as a template (Protein Data Bank number 1UBW (29)), a homology model of TbFPPS was built using default settings in the Modeler module of Insight II (30). The majority of models constructed in this way were immediately discounted because of energy considerations and restraint violations, leaving a small group of structures that was further evaluated using the Procheck program (31). In the reported model, the number of residues in the most favored region of the Ramachandran plot and the overall G-factor were significantly better than typical for 2.6-Å resolution structures (91% and 0.0, respectively). This, together with the fact that the root mean square deviation of the homology model from the template for non-loop atoms was only 0.41 Å, lends confidence to the quality of the reported structure.

To model GPP in the TbFPPS active site, we transferred the GPP coordinates from the template model into the TbFPPS structure. This resulted in steric clashes between GPP and Tyr$^{99}$, because the template residue for Tyr$^{99}$ in the avian crystal structure is a F113S mutant and so provides little information about the side chain geometry of Tyr$^{99}$. To correct this, the geometries of His$^{98}$ and Tyr$^{99}$ were therefore optimized, because the template for His$^{98}$ is also a mutant (F112A) and hence also lacks important side chain information. Rotamer searches for His$^{98}$ and Tyr$^{99}$ were performed to minimize the GPP-Tyr$^{99}$ and His$^{98}$-Tyr$^{99}$ interactions. Hydrogen atoms were added within Insight II to simulate a pH of 7.0, and GPP was taken to be deprotonated. CHARMM27 potentials and partial charges were applied to all atoms, except for the vinylic hydrogens in GPP, which were set manually. Charges for GPP were obtained using the Gaussian 98 program (32), using the x-ray coordinates of GPP to calculate Merz-Singh-Kollman charges at the HF/6–31++G** level. The coordinates of His$^{98}$ and Tyr$^{99}$ were then optimized by using 1000 steps of steepest descents minimization, then further optimized by using the conjugate gradient algorithm to a gradient tolerance of 0.0001 kcal mol$^{-1}$ Å$^{-1}$. This structure was then uploaded to the Consurf server[3] and Rasmol (33) was used to visualize the three-dimensional locations of highly conserved residues in the TbFPPS model.

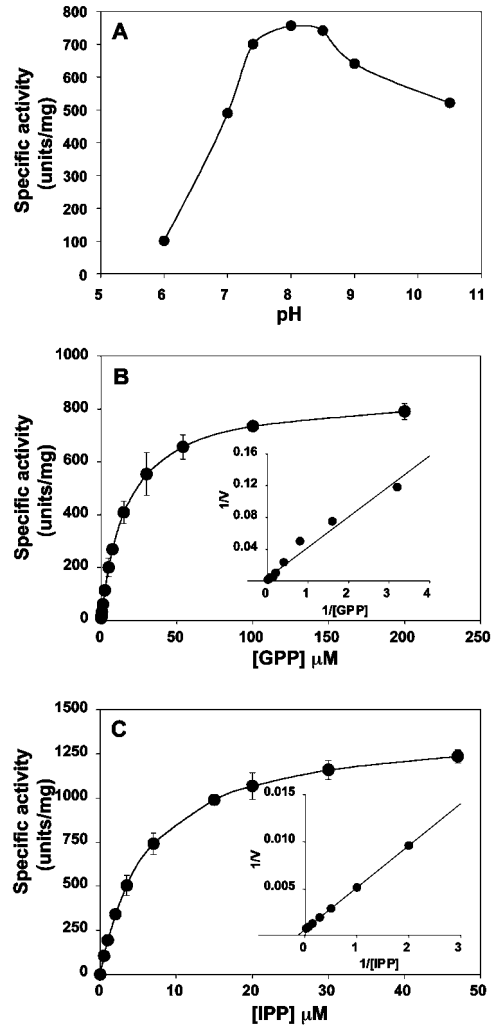


FIG. 4. **Effect of pH and substrate concentration on FPPS activity.** FPPS activity was measured as described under "Experimental Procedures" over a range of pH between 6 and 10.5 using Tris-HCl and Tris glycine buffers (*A*), and in the presence of different concentrations of GPP (*B*) or IPP (*C*). *Insets* in *B* and *C* represent the linear transformation, by double reciprocal plot, of each curve.

To further understand the activities of the bisphosphonates investigated (Fig. 1), we applied pharmacophore modeling techniques to the

[3] F. Glaser, T. Pupko, I. Paz, R. E. Bell, D. Bechor, E. Martz, and N. Ben-Tal, www.consurf.tau.ac.il.

TbFPPS inhibition results discussed later. The HipHop module in Catalyst 4.6 (34) was used to identify the spatial relationships of the chemical features common to the most active models. Compounds **1**, **2**, **3**, **4**, and **5** (Fig. 1) were used in pharmacophore generation, because only these compounds were identified as "active" by Catalyst default settings. Up to 255 best quality conformations of each compound were built using the Confirm module in Catalyst 4.6. We allowed models to contain two negative ionizable features, one positive charge feature, and one custom endocyclic carbon atom feature, as input for pharmacophore generation. Although HipHop did not identify any pharmacophore that could map all four features in each compound, a suitable hypothesis that did identify these features was found by merging two HipHop models.

For comparison purposes, *T. brucei* cell growth inhibition data (4) was used to build a quantitative pharmacophore model using the Hypogen module in Catalyst 4.6 (34). For this model, we used the same features as in the TbFPPS analysis, but pharmacophores found in this way did not adequately describe the activities of the aliphatic bisphosphonates. To account for these compounds, a hydrophobic aliphatic feature was added to the Hypogen pharmacophore to describe long chain compounds. The endocyclic carbon feature was modified to also identify terminal methyl carbon atoms in short side chains (less than 6 heavy atoms long), thus accounting for the increased potency of olpadronate with respect to pamidronate. This pharmacophore gave good correlation between predicted and experimental $IC_{50}$ values, with $R^2$ = 0.68 (data not shown).

## RESULTS

*Cloning of the TbFPPS Gene*—To screen for genes encoding FPPS in *T. brucei*, the amino acid sequence of *T. cruzi* FPPS (AF312690) was used to search the *T. brucei* data base of The Institute for Genome Research (TIGR) using tBLASTn. This search yielded six *T. brucei* genomic survey sequence clones. The predicted amino acid sequence encoded by clone 6A5 (accession number AQ651702) contained the C terminus of this protein. The fragment of the *T. brucei* FPPS gene was amplified by PCR using oligonucleotide primers complementary to the genomic survey sequence with genomic *T. brucei* DNA acting as a template. The product of the amplification (428 bp) was ligated into vector pCR2.1TOPO for sequence analysis. This sequence enabled appropriate gene-specific primers to be designed for the generation of 5′-end and 3′-end DNA fragments using the 5′-rapid amplification of cDNA ends method (35) and reconstruction of a full-length cDNA. The nucleotide sequence of 2070 bp revealed an open reading frame of 1101 bp, which encodes a 367-amino acid protein with a predicted molecular mass of 42 kDa. Two oligonucleotide primers based in the 5′- and 3′-untranslated regions of this gene were then used to amplify the open reading frame from genomic *T. brucei* DNA, to obtain a genomic clone. The open reading frame was identical with the full-length cDNA. A BLAST search of the protein data base showed that the amino acid sequence from *T. brucei* has 32–68% identity and 50–81% similarity with other representative FPPS. The amino acid sequence of the *T. brucei* enzyme was aligned with the sequences of *T. cruzi*, human, and *Saccharomyces cerevisiae* FPPSs as shown in Fig. 2*A*. All residues involved in catalysis or binding (regions I–VII) identified in other FPPSs (36) are present in the *T. brucei* enzyme.

A CLUSTALW alignment of FPPS peptide sequences from avian, some mammalian, fungal, plant, and bacterial FPPSs was then used as the basis for the generation of a phylogentic tree (Fig. 2*B*). The results suggested that *T. brucei* and *T. cruzi* enzymes shared a most recent common ancestor. *Plasmodium falciparum* and fungal and plant FPPSs were the closest outgroups to the trypanosomatid sequences.

Southern blot analysis was performed with a PCR fragment that encompasses the entire coding region of *TbFPPS* (Fig. 3*A*). Digestions with enzymes that cut at sites not contained within the coding region of the gene gave single bands (*Eco*RI, *HindIII*, *Xho*I), whereas two bands were obtained with enzymes with unique restriction sites in the open reading frame (*Kpn*I, *Spe*I, *Ava*I, *Hinc*II, *Nsi*I), suggesting that the gene was single copy per haploid genome.

TABLE II
*The effects of bisphosphonates on FPPS activity*

The activity of the *T. brucei* enzyme was assayed in the presence of bisphosphonates in mixtures containing 10 mM Hepes (pH 7.4), 5 mM $MgCl_2$, 2 mM dithiothreitol, 47 μM 4-[$^{14}$C]IPP (10 μCi/μmol), 54 μM GPP, and 10 ng of protein in a final volume of 100 μl. Reactions were incubated for 30 min at 37°C and the prenyl product was extracted and measured by liquid scintillation counting.

| Inhibitor | *T. brucei* FPPS | |
|---|---|---|
| | $K_i$[a] | $IC_{50}$[a] |
| | μM | |
| 1 | 0.007 ± 0.0006 | 0.046 ± 0.003 |
| 2 | 0.010 ± 0.002 | 0.054 ± 0.003 |
| 3 (Risedronate) | 0.010 ± 0.002 | 0.042 ± 0.002 |
| 4 (Incadronate) | 0.011 ± 0.002 | 0.035 ± 0.009 |
| 5 | 0.058 ± 0.022 | 0.15 ± 0.047 |
| 6 (Pamidronate) | 0.40 ± 0.12 | 1.2 ± 0.24 |
| 7 | 0.57 ± 0.07 | 3.5 ± 0.41 |
| 8 | 1.3 ± 0.16 | 4.9 ± 0.06 |
| 9 | 8.5 ± 4.3 | 28 ± 10.4 |
| 10 | | 105 |

[a] Values are the mean ± S.D. of three independent experiments in duplicate.

*Purification and Reaction Requirements of Recombinant Protein*—*TbFPPS* was expressed in *E. coli* BL21(DE3) as a fusion protein with an N-terminal polyhistidine tag. Affinity chromatography on nickel-chelated agarose permitted a simple, one-step purification. Enzyme purity was judged by using SDS-PAGE with Coomassie Blue staining (Fig. 3*B*). The final protein preparation catalyzed the incorporation of 4-[$^{14}$C]IPP into a hexane-extractable material when the allylic substrates, dimethylallyl pyrophosphate and GPP, were used (data not shown) (17). 4-[$^{14}$C]IPP incorporation into the organic solvent extractable material was linear with time for at least 60 min. The radioactive assay was performed in the presence of different concentrations of $Mg^{2+}$ and $Mn^{2+}$, to determine their effect on the *T. brucei* FPPS. $Mg^{2+}$ and $Mn^{2+}$ were added to the reaction mixture at concentrations between 0.5 and 20 mM. As shown in Table I, optimal levels of activity were obtained by the addition of 5–10 mM $Mg^{2+}$. Enzyme activity was very low when the divalent cation was $Mn^{2+}$. The addition of 10 mM EDTA abolished FPPS activity. Enzyme activity was also assayed between pH 6 and 10.5 using a Tris-HCl (10 mM)/Tris glycine (10 mM) buffer. Optimum activity was observed between pH 7.4 and 8.5 (Fig. 4*A*).

*Kinetic Analysis*—Standard procedures were used to determine kinetic parameters. $K_m$ and $V_{max}$ values were obtained by a non-linear regression fit of the data to the Michaelis-Menten equation (SigmaPlot 2000 for Windows). When the rate of FPP synthesis by the recombinant enzyme (10 ng) was measured in the presence of saturating IPP (47 μM) and varying GPP concentration between 0.15 and 200 μM, a $K_m$ value of 17.2 ± 3.9 μM and a $V_{max}$ value of 857.0 ± 8.7 units/mg, were calculated (Fig. 4*B*). When the concentration of GPP was kept at 200 μM and the IPP concentration was varied between 0.5 and 47 μM, the $K_m$ value was 6.2 ± 0.6 μM and the $V_{max}$ was 1,399.7 ± 1.3 units/mg (Fig. 4*C*).

*Inhibition by Bisphosphonates*—Nine bisphosphonates (**1**–**9**) together with the bromohydrin of isopentenylpyrophosphate (Phosphostim, **10**), shown in Fig. 1, were tested for their ability to inhibit the *T. brucei* enzyme. $K_i$ values were calculated by using the Dixon equation (37) and the $IC_{50}$ values were obtained as described previously (17) (Table II). BPs are known competitive inhibitors with respect to GPP of FPPSs of different origins (15).

*RNA Interference*—The essentiality of *TbFPPS* was investi-

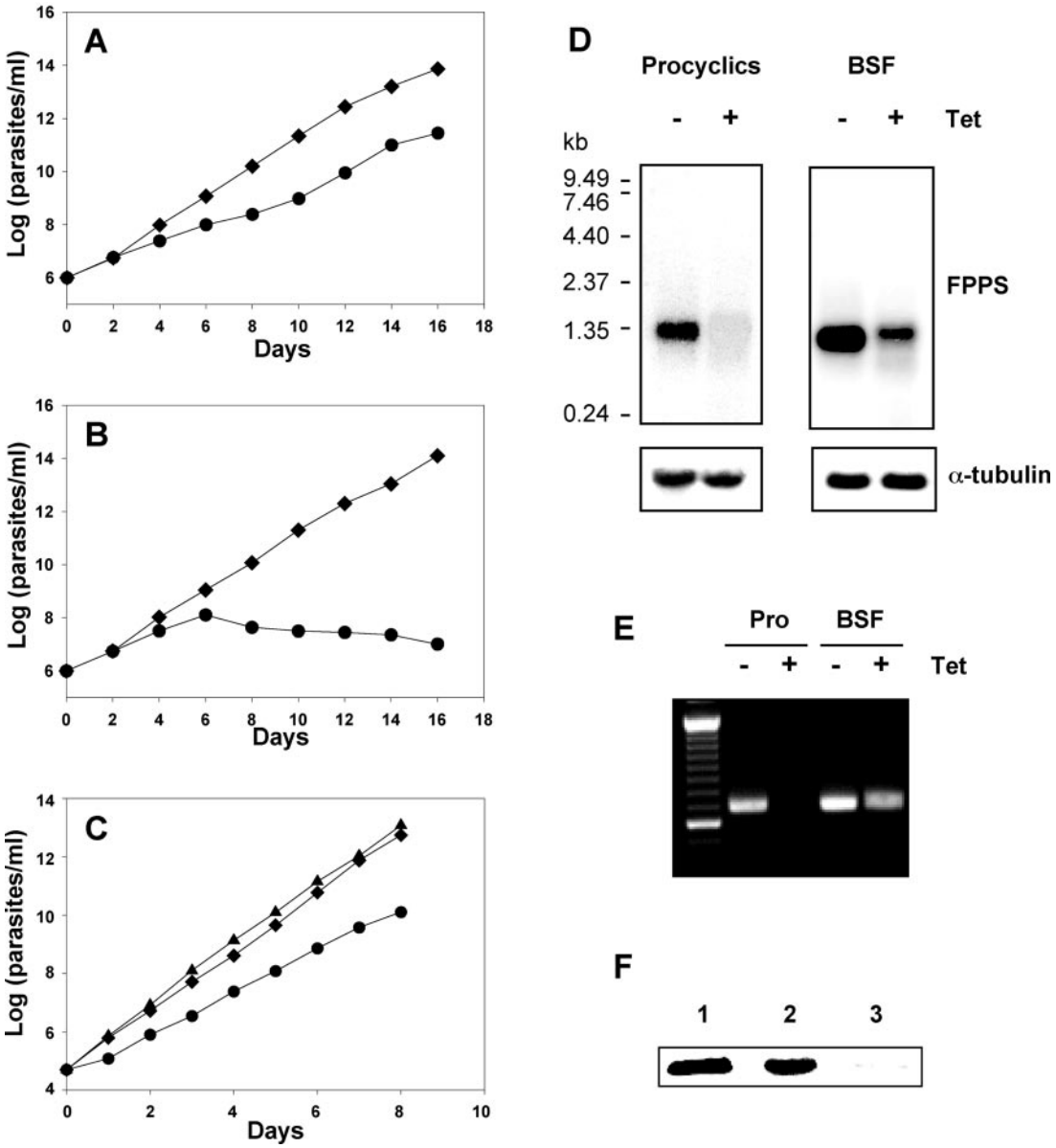


FIG. 5. **Effects of inhibition of TbFPPS expression by tetracycline-inducible double-stranded RNA on cell growth.** Procyclic form RNAi constructs grown in medium supplemented with 15% FBS (*A*) or 15% dialyzed FBS (*B*). Cells were grown in the absence (*diamonds*) or presence of tetracycline (1 μg/ml) (*circles*). *C*, bloodstream forms grown in medium supplemented with 10% FBS or 5% dialyzed FBS and 10% Serum Plus in the absence (*triangles* and *diamonds*, respectively) or presence of tetracycline (1 μg/ml) (*circles*). *D*, Northern blot analysis of *TbFPPS* RNA from procyclic and bloodstream forms (*BSF*) grown in the absence (−) or presence (+) of tetracycline (*Tet*). Total RNA was subjected to gel electrophoresis before transfer to a nylon membrane, then hybridized with the $^{32}$P-labeled probe corresponding to the FPPS coding sequence. As a control, these blots were also reprobed with α-tubulin. *E*, RT-PCR analysis of total RNA from procyclic (*Pro*) and bloodstream forms using primers specific for the TbFPPS. The cells were grown in the absence (−) or presence (+) of tetracycline and dialyzed FBS for 24 h. *F*, immunoblot analysis of *T. brucei* procyclic form lysates (30 μg of protein/lane) from uninduced parasites on days 0 (*lane 1*) and 4 (*lane 2*) of the culture, and tetracycline-induced cells for 4 days (*lane 3*).

gated by using RNAi. The inactivating fragment for RNAi was inserted between the two opposing T7 promoters of the pZJM vector that are both regulated by tetracycline repressors (18). Transfection of the procyclic and bloodstream forms of *T. brucei* that express the tetracycline repressor and the bacterial T7 RNA polymerase with RNAi constructs directed against *TbFPPS* resulted in cells that survived phleomycin selection. When production of double-stranded RNA was induced by tetracycline in procyclic forms grown in medium supplemented with 15% FBS, cell growth decreased as compared with non-induced parasites after day two (Fig. 5*A*). When the induction of RNAi was performed in a medium supplemented with 15% dialyzed FBS, instead of normal FBS, the parasites' growth rate declined after 2 days of tetracycline induction, and the cells subsequently died (Fig. 5*B*). Northern blot analysis of *TbFPPS* RNA from cells grown with 15% dialyzed FBS in the absence or presence of tetracycline for 24 h showed reduction of intact *TbFPPS* RNA and a broad smear that probably represents degraded RNA (Fig. 5*D*). No mRNA could be found in these parasites as analyzed by RT-PCR (Fig. 5*E*). Immunoblot analysis using an affinity-purified antiserum raised against *T. cruzi* FPPS (17) detected a band of 43.9 kDa in procyclic form lysates, which is very close to the size predicted by its amino acid sequence (42 kDa). This band was not detected in the RNAi-induced cells by day 4 (Fig. 5*F*, *lane 3*). Induction of *TbFPPS* double stranded RNA in bloodstream forms caused an inhibition of cell proliferation, but they still exhibited exponential growth even when cultured in the presence of dialyzed serum

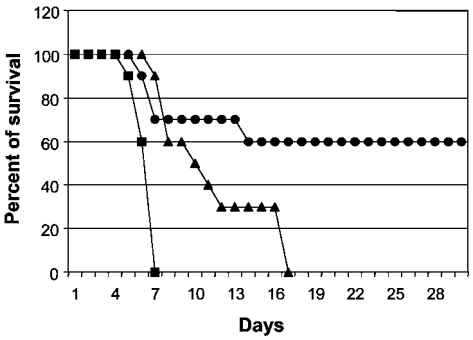


FIG. 6. **Survival data for *T. brucei brucei*-infected mice.** *Squares*, control group (infected, untreated); *triangles*, treated group, 10 mg/kg intraperitoneal, ×5; *circles*, treated group, 2× 5 mg/kg per day intraperitoneal, for 5 days.

(Fig. 5*C*, *circles*). When mRNA levels were analyzed by Northern blot (Fig. 5*D*) or RT-PCR (Fig. 5*E*), the target mRNA was still detectable after addition of the antibiotic. Western blot analysis also detected the presence of the TbFPPS protein (data not shown).

*Treatment of T. brucei-infected Mice with Bisphosphonates*—We tested six bisphosphonates (**1**, **2**, **3**, **6**, **7**, and **8**) for FPPS inhibition activity on mice infected with *T. brucei* strain 427, variant 117. This strain gives an acute lethal infection in mice 5–6 days after infection with 10,000 trypomastigotes. Risedronate was first tested at doses of 5 mg/kg for 5 days and 10 mg/kg for 5 days, giving one dose per day. There was no significant protection against death except for some delay in the death of the animals at a 10 mg/kg for 5 days (one mouse died at day 7, one at day 8, one at day 9, one at day 12, and one at day 17; all controls died at day 6) (Fig. 6). Increasing the dose to 10 mg/kg for 7 days or 15 mg/kg for 5 days resulted in toxicity, as indicated by excessive panting and horripilation, and the animals died at the same time as the controls. However, using a split dose regime (2× 5 mg/kg per day) for 5 days there was a 60% survival (one mouse died at day 7, another at day 14, whereas 3 mice survived more that 3 months without parasitemia). All mice treated with the standard drug pentamidine (4 mg/kg for 4 days) survived more than 3 months without parasitemia. Compounds **1**, **2**, **7**, and **8** were also investigated at a dose of 10 mg/kg for 5 days (single or split dose regiment) but there was toxicity, and no protection against death was observed. Pamidronate (10 mg/kg intraperitoneal × 5 days) was also ineffective.

*Homology Modeling*—We used the sequence information of TbFPPS together with the known three-dimensional x-ray crystallographic structure of the avian FPPS enzyme (29) to obtain the homology model of the TbFPPS protein shown in Fig. 7*A*. In both the *T. brucei* and *T. cruzi* proteins, there is an 11-mer insertion sequence (residues 184–194 in the *T. brucei* sequence), which is shown highlighted in *yellow* on the *left* of Fig. 7*A*. In addition, the *T. brucei* sequence contains a second insertion, shown in *yellow* on the *right* of Fig. 7*A*. The functions of these loops are not known. However, it is of interest to note that of some 20 FPPS investigated, only the trypanosomatid parasites and, apparently, *Plasmodium falciparum* (38) contain such insertions, and it is possible that these loops may play a role in FPPS function in these organisms. As can be seen in Fig. 7, this sequence and homology modeling information can also be used to construct a three-dimensional picture of the conserved nature of each residue in TbFPPS (Fig. 7*B*). Here, we show a color-coded "consensus" picture of different FPPSs: the most highly conserved residues are coded *mauve*, followed by decreasing conservation: *dark pink* > *light pink* > *blue* > *cyan* > *white*. The GPP substrate is docked into the hybrophobic cleft or active site region, which for the most part is highly conserved across species (*mauve* color). There are, however, some interesting differences between the trypanosomatid and other FPPS sequences investigated, in particular, the FF or YF residues located toward the distal end of the hydrophobic pocket of most FPPSs (at positions 98 and 99) are changed to HY in both the *T. cruzi* and *T. brucei* proteins (and to SF in *P. falciparum*), offering some potential for the development of novel inhibitors that might hydrogen bond to these residues.

*Structure-Activity Investigation*—To begin to carry out a three-dimensional structure-activity relationship investigation of TbFPPS inhibition by the compounds investigated, we utilized the Catalyst™ technique (34). The Catalyst™ program basically explores a wide range of conformations (up to 255) for a given molecule and correlates particular spatial features with observed experimental activity. In this way, a pharmacophore can be generated that contains specific chemical features (such as aromatic groups, positive charges, hydrogen bond donors/acceptors, and negative ionizable groups) in specific locations, which correlate with activity. When large amounts of $K_i$ information are available, a quantitative structure-activity relationship model can be developed, whereas for a smaller data set, such as that we have obtained, the pharmacophore contains the major features of importance in enzyme inhibition, but is less suitable for quantitative predictions. Using this approach (the HipHop feature in Catalyst™) we obtained the pharmacophore shown in Fig. 8, *A–C*. This pharmacophore contains four features of key importance in drug activity: two negative ionizable groups (the bisphosphonates, shown in *blue*); an endocyclic carbon (*green*) and a positive charge (red). These features are shown superimposed on the stick diagram structures of two of the more active species: 3-picolylaminomethylene bisphosphonate **1** (Fig. 8*A*) and risedronate (**3**, Fig. 8*B*). The pharmacophore is also shown docked into the active site of TbFPPS (+GPP) in Fig. 8*C*.

Next, we used the Catalyst™ approach to develop a pharmacophore for *in vitro T. brucei* growth inhibition, using data obtained previously (4), to compare with the enzyme inhibition results. In this case, test results for some 26 compounds are available, which enables use of the more quantitative Hypogen feature of Catalyst™. Using Hypogen, we obtained a pharmacophore for *T. brucei* growth inhibition that is quite similar to that obtained for TbFPPS enzyme inhibition (obtained using HipHop). This similarity can clearly be seen in Fig. 8*D* in which we show, superimposed, the pharmacophores for enzyme inhibition and for *T. brucei* cell growth inhibition. The *T. brucei* growth inhibition model contains an additional custom hydrophobic feature to account for, in a quantitative manner, the activity of the long chain *n*-alkyl bisphosphonates (4).

## DISCUSSION

The sensitivity of trypanosomatid protozoa to isoprenoid biosynthesis inhibitors (39) offers a unique opportunity for drug target identification and the subsequent development of new anti-trypanosomatid agents. FPPS plays a central role in metabolism through the enzymatic generation of FPP, which is used for protein prenylation, and for the synthesis of sterols, dolichols, heme *a*, and ubiquinone, and is potently inhibited by bisphosphonates (11–16). Stringent genetic validation of putative drug targets is desirable before the rational design of inhibitory compounds intended for chemotherapeutic use is undertaken (40). This study validates FPPS as a drug target through the use of RNAi studies. It provides genetic evidence that FPPS plays an essential cellular role in *T. brucei* and demonstrates that the enzyme is vital for parasite survival *in vitro* and *in vivo*. The finding that a similar pharmacophore can be obtained by structure-activity investigations of *in vitro*

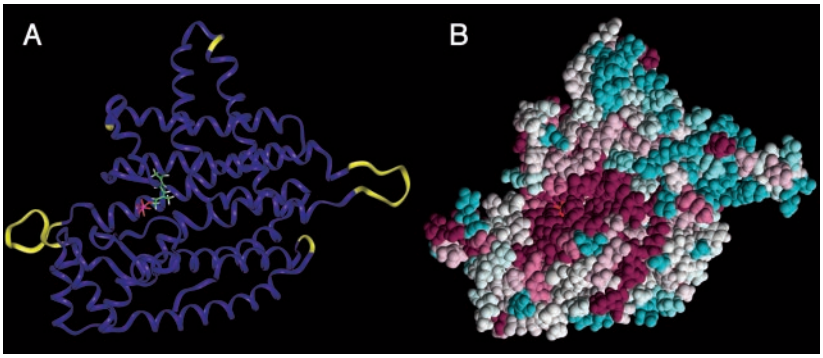


FIG. 7. **Molecular models of TbFPPS.** *A*, TbFPPS homology model based on template avian x-ray structure of FPPS + GPP (Protein Data Bank number 1UBW). The leftmost insertion (loop) shown in *yellow* has only been found in protozoan parasites. *B*, Consurf model illustrates sequence variability. The color coding illustrates conservation in the following order: *white* (highly variable) < *cyan* < *blue* < *light pink* < *dark pink* < *mauve* (highly conserved).

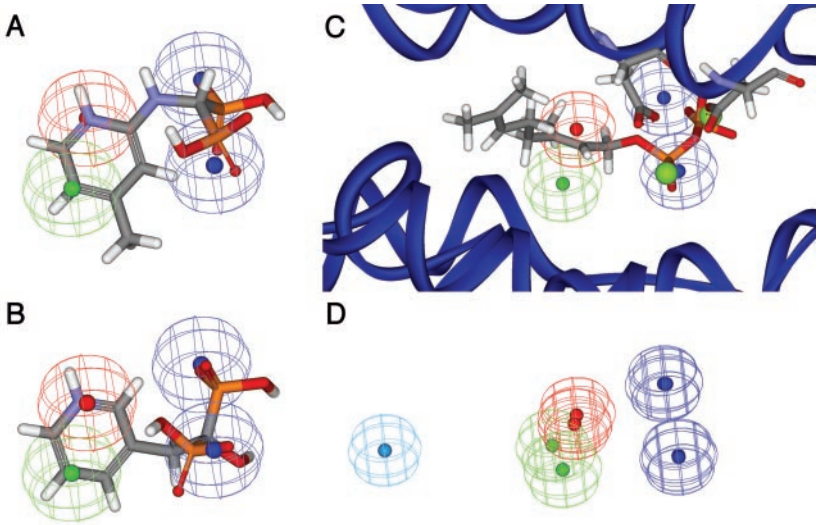


FIG. 8. **Pharmacophore models for TbFPPS inhibition (*A–C*) and *T. brucei* cell growth inhibition (*D*).** In *A*, the HipHop pharmacophore is shown superimposed on **1**, in *B* on risedronate (**3**), in *C* it is docked onto GPP in the TbFPPS active site. *D* shows the HipHop pharmacophore superimposed on the Hypogen pharmacophore for *T. brucei* growth inhibition (data from Ref. 34). Graphics were generated with the Accelrys ViewerLite program (www.accelrys.com).

growth and enzyme inhibition data further validates TbFPPS as the target of bisphosphonates.

The *T. brucei* FPPS gene, *TbFPPS*, was shown to be present in the *T. brucei* genome and encodes for a functional enzyme. As shown in the alignment in Fig. 2*A*, there is considerable sequence similarity between different FPPSs. Heterologous expression of *TbFPPS* in *E. coli* resulted in the production of a recombinant enzyme that was generally similar to other FPPSs with respect to its $Mg^{2+}$ requirement, optimum pH, and sensitivity to bisphosphonates. As shown in Table I and Fig. 4*A*, the protein we have expressed has optimum activity in the presence of 0.5–10 mM $MgCl_2$ and in the pH range 7.4–8.5, basically as found with the human enzyme (41). In addition, our results show that TbFPPS is potently inhibited by a number of bisphosphonates (Table II). The most potent inhibitor found is the aminomethylene bisphosphonate **1**, having a $K_i$ of 7 nM, followed closely by its isomer **2** and risedronate (**3**), both of which have $K_i$ = 10 nM. The next most potent inhibitors found were the drugs incadronate (**4**, $K_i$ = 11 nM), the isoquinoline species (**5**, $K_i$ = 58 nM), and pamidronate (**6**, $K_i$ = 400 nM). The general pattern of reactivity found here is similar to that found for bisphosphonate inhibition of a recombinant human FPPS, where the activity profile is again risedronate > incadronate > pamidronate (42). Likewise, the picolyl aminomethylene bisphosphonate **2** has been found to be a potent ($IC_{50}$ = 25 nM) inhibitor of a plant FPPS (11) and this species is also a potent inhibitor of bone resorption (43), consistent with activity *versus* human FPPS. The imidazo(1,2-*H*)pyridyl species **9** is relatively inactive, consistent with its poor performance as a bone antiresorptive agent (19), presumably because of unfavorable steric interactions in the TbFPPS active site.

In addition to these investigations of aromatic bisphosphonate inhibitors, we also tested whether aliphatic, nitrogen-free bisphosphonates might act as inhibitors of TbFPPS, because these compounds have been found to have activity against the growth of both *T. cruzi* and *Entamoeba histolytica*, *in vitro* (44, 45). The bisphosphonates **7** and **8** contain simple *n*-alkyl side chains containing 10 and 11 carbon atoms, and were found to have $K_i$ values of 0.57 and 1.3 $\mu$M, respectively. These $K_i$ values are still quite small and approach those found with second generation bone resorption drugs such as pamidronate ($K_i$ = 0.40 $\mu$M, Table II). Indeed, in very early work, Shinoda *et al.* (46) proposed that species such as **7** and **8** might be used in treating bone resorption diseases. Presumably, although these species do not contain the ammonium or pyridinium-like features associated with the most potent inhibitors, they do provide an enhanced hydrophobic interaction (van der Waals dispersion) in the active site of the enzyme, resulting in at least moderate activity. The importance of this effect is also seen on transition from pamidronate to olpadronate to ibandronate (47), where successive *N*-alkylations and chain elongations result in a potent FPPS inhibitor, having an $IC_{50}$ of 20 nM against a human recombinant FPPS (42). The slightly increased $K_i$ for the longer chain species is not inconsistent with this idea, because it has recently been shown by the Novartis group (48) that increasing the side chain length of *N*-containing bisphosphonates beyond a certain threshold basically abolishes all activity, most likely because they clash with the aromatic rings located at the distal end of the hydrophobic pocket, thought to be responsible for termination of isoprene chain elongation by FPPS (29). In any case, it is of interest that the simple alkyl species **7** has essentially the same activity as pamidronate.

We also tested the activity of one pyrophosphate species, the bromohydrin of isopentenylpyrophosphate, **10**. This compound

is currently being developed as an anti-cancer drug and is known to stimulate the growth and cytokine expression of γδ T cells (49), but its precise molecular mechanism of action is unclear. Because FPPS, in addition to its direct role in FPP synthesis, is also known to be involved in binding to the tyrosine kinase domain of the fibroblast growth factor receptor (50) and affects cell growth, it seemed possible that this alternative role of FPPS might also occur in γδ T cells, mediated by pyrophosphate (and indeed, bisphosphonate (51, 52)) binding. We therefore determined the $K_i$ for the bromohydrin pyrophosphate, **10**. We obtained a $K_i = 103\ \mu$M, which would tend not to support this possibility.

This leads us finally to consider the potential use of these and related compounds in chemotherapeutic intervention. Here, our initial results indicated that procyclic (insect form) trypomastigotes were extremely sensitive to the effects of RNAi, which generated a lethal phenotype. In the bloodstream forms, RNAi only slowed growth, and was not lethal. However, this was because of the leakiness of the vector in these forms, because the mRNA was not completely eliminated after induction of cells with tetracycline. Consequently, we carried out a series of *in vivo* tests of selected bisphosphonates (**1**, **2**, **3**, **6**, **7**, and **8**) *versus T. brucei*-infected mice. The most effective compound tested was risedronate (**3**), which afforded a 60% cure (survival of 3/5 mice) at a dose of 2 × 5 mg/kg per day for 5 days, intraperitoneally (Fig. 6). This clearly demonstrates that bisphosphonates can effectively suppress parasite proliferation *in vivo* as well as *in vitro* and that bisphosphonates may thus be useful lead compounds for the synthesis of new drugs effective against African sleeping sickness.

*Acknowledgments*—We thank G. A. M. Cross (Rockefeller University) for generously providing trypanosome strains 29-13 and BF, P. Englund (Johns Hopkins University) for the RNAi vector pZJM, and Linda Brown for technical assistance. Preliminary sequence data for the *T. brucei* genomic survey sequence (GenBank™ accession number AQ651702) was obtained from The Institute for Genomic Research website.

REFERENCES

1. Barrett, M. P. (1999) *Lancet* **353,** 1113–1114
2. Dumas, M., and Boutelle, B. (2000) *Bull. W.H.O.* **78,** 9–12
3. Martin, M. B., Grimley, J. S., Lewis, J. C., Heath, H. T., III, Bailey, B. N., Kendrick, H., Yardley, V., Caldera, A., Lira, R., Urbina, J. A., Moreno, S. N. J., Docampo, R., Croft, S. L., and Oldfield, E. (2001) *J. Med. Chem.* **44,** 909–916
4. Martin, M. B., Sanders, J. M., Kendrick, H., de Luca-Fradley, K., Lewis, J. C., Grimley, J. S., Van Brussel, E. M., Olsen, J. R., Meints, G. A., Burzynska, A., Kafarski, P., Croft, S. L., and Oldfield, E. (2002) *J. Med. Chem.* **45,** 2904–2914
5. Yardley, V., Khan, A. A., Martin, M. B., Slifer, T. R., Araujo, F. G., Moreno, S. N. J., Docampo, R., Croft, S. L., and Oldfield, E. (2002) *Antimicrob. Agents Chemother.* **46,** 929–931
6. Rodriguez, N., Bailey, B. N., Martin, M. B., Oldfield, E., Urbina, J. A., and Docampo, R. (2002) *J. Infect. Dis.* **186,** 138–140
7. Rogers, M. J., Watts, D. J., and Russell, R. G. G. (1997) *Cancer* (*Suppl.*) **80,** 1652–1660
8. Rodan, G. A. (1998) *Annu. Rev. Pharmacol. Toxicol.* **38,** 375–388
9. Brown, D. L., and Robbins, R. (1999) *J. Clin. Pharmacol.* **39,** 1–10
10. Rodan, G. A., and Martin, T. J. (2000) *Science* **289,** 1508–1514
11. Cromartie, T. H., Fisher, K. J., and Grossman, J. N. (1999) *Pest. Biochem. Physiol.* **63,** 114–126
12. Martin, M. B., Arnold, W., Heath, H. T., Urbina, J. A., and Oldfield, E. (1999) *Biochem. Biophys. Res. Commun.* **263,** 754–758
13. van Beek, E., Peterman, E., Cohen, L., Löwik, C., and Papapoulos, S. (1999) *Biochem. Biophys. Res. Commun.* **264,** 108–111
14. Keller, R. K., and Fiesler, S. J. (1999) *Biochem. Biophys. Res. Commun.* **266,** 560–563
15. Bergstrom, J. D., Bostedor, R. G., Masarachia, P. J., Reszka, A. A., and Rodan G. (2000) *Arch. Biochem. Biophys.* **373,** 231–241
16. Grove, J. E., Brown, R. J., and Watts, D. J. (2000) *J. Bone Miner. Res.* **15,** 971–981
17. Montalvetti, A., Bailey, B. N., Martin, M. B., Severin, G. W., Oldfield, E., and Docampo, R. (2001) *J. Biol. Chem.* **276,** 33930–33937
18. Morris, J. C., Wang, Z., Drew, M. E., Paul, K. S., and Englund, P. T. (2001) *Mol. Biochem. Parasitol.* **117,** 111–113
19. Takeuchi, M., Sakamoto, S., Kawamuki, K., Kurihara, H., Nakahara, H., and Isomura, Y. (1998) *Chem. Pharm. Bull.* **46,** 1703–1709
20. Belmant, C., Fournié, J. J., Bonneville, M., and Peyrat, M. A. (2000) French Patent 2,782,721
21. Wirtz, E., Leal, S., Ochatt, C., and Cross, G. A. (1999) *Mol. Biochem. Parasitol.* **99,** 89–101
22. Hirumi, H., and Hirumi, K. (1989) *J. Parasitol.* **75,** 985–989
23. Thompson, J. D., Higgins, D. G., and Gibson, T. J. (1994) *Nucleic Acids Res.* **22,** 4673–4680
24. Felsenstein, J. (1989) *Cladistics* **5,** 164–166
25. Saitou, N., and Nei, M. (1987) *Mol. Biol. Evol.* **4,** 406–425
26. Wang, Z., Morris, J. C., Drew, M. E., and Englund, P. T. (2000) *J. Biol. Chem.* **275,** 40174–40179
27. Hill, J. E., Scott, D. A., Luo, S., and Docampo, R. (2000) *Biochem. J.* **351,** 281–288
28. Bradford, M. M. (1976) *Anal. Biochem.* **72,** 248–254
29. Tarshis, L. C., Proteau, P. J., Kellogg, B. A., Sacchettini, J. C., and Poulter, C. D. (1996) *Proc. Natl. Acad. Sci.* **93,** 15018–15023
30. Accelrys, Inc. (2002) *Insight II Program 2000.1*, Accelrys, Inc., San Diego, CA
31. Laskowski, R. A., MacArthur, M. W., Moss, D. S., and Thornton, J. M. (1993) *J. Appl. Crystallogr.* **26,** 283–291
32. Frisch, M. J., Trucks, G. W., Schlegel, H. B., Scuseria, G. E., Robb, M. A., Cheeseman, J. R., Zakrzewski, V. G., Montgomery, J. A., Jr., Stratmann, R. E., Burant, J. C., Dapprich, S., Millam, J. M., Daniels, A. D., Kudin, K. N., Strain, M. C., Farkas, O., Tomasi, J., Barone, V., Cossi, M., Cammi, R., Mennucci, B., Pomelli, C., Adamo, C., Clifford, S., Ochterski, J., Petersson, G. A., Ayala, P. Y., Cui, Q., Morokuma, K., Malick, D. K., Rabuck, A. D., Raghavachari, K., Foresman, J. B., Cioslowski, J., Ortiz, J. V., Baboul, A. G., Stefanov, B. B., Liu, G., Liashenko, A., Piskorz, P., Komaromi, I., Gomperts, R., Martin, R. L., Fox, D. J., Keith, T., Al-Laham, M. A., Peng, C. Y., Nanayakkara, A., Challacombe, M., Gill, P. M. W., Johnson, B., Chen, W., Wong, M. W., Andres, J. L., Gonzalez, C., Head-Gordon, M., Replogle, E. S., and Pople, J. A. (1998) *Gaussian 98*, *Revision A. 9*, Gaussian, Inc., Pittsburgh, PA
33. Sayle, R. A., and Milner-White, E. J. (1995) *Trends Biochem. Sci.* **20,** 374–376
34. Accelrys, Inc. (2000) *Catalyst 4.6 Program*, Accelrys, Inc., San Diego, CA
35. Frohman, M. A., Dush, M. K., and Martin, G. R. (1988) *Proc. Natl. Acad. Sci. U. S. A.* **85,** 8998–9002
36. Koyama, T. (1999) *Biosci. Biotechnol. Biochem.* **63,** 1671–1676
37. Dixon, M. (1972) *Biochem. J.* **129,** 197–202
38. Gardner, M. J., Hall, N., Fung, E., White, O., Berriman, M., Hyman, R. W., Carlton, J. M., Pain, A., Nelson, K. E., Bowman, S., Paulsen, I. T., James, K., Eisen, J. A., Rutherford, K., Salzberg, S. L., Craig, A., Kyes, S., Chan, M.-S., Nene, V., Shallom, S. J., Suh, B., Peterson, J., Angiuoli, S., Pertea, M., Allen, J., Selengut, J., Haft, D., Mather, M. W., Vaidya, A. B., Martin, D. M. A., Fairlamb, A. H., Fraunholz, M. J., Roos, D. S., Ralph, S. A., McFadden, G. I., Cummings, L. M., Subramaian, G. M., Mungall, C., Venter, J. C., Carucci, D. J., Hoffman, S. L., Newbold, C., Fraser, C. M., and Barell, B. (2002) *Nature* **419,** 498–511
39. Docampo, R., and Moreno, S. N. J. (2001) *Current Drug Targets Infectious Disorders* **1,** 51–61
40. Wang, C. C. (1997) *Parasitology* **114,** S31–S44
41. Ding, V. D.-H., Sheares, B. T., Bergstrom, J. D., Ponpipom, M. M., Perez, L. B., and Poulter, C. D. (1991) *Biochem. J.* **275,** 61–65
42. Dunford, J. E., Thompson, K., Coxon, F. P., Luckman, S. P., Hahn, F. M., Poulter, C. D., Ebetino, F. H., and Rogers, M. J. (2001) *J. Pharmacol. Exp. Ther.* **296,** 235–242
43. Sunberg, R. J., Ebetino, F. H., Mosher, C. T., and Roof, C. F. (1991) *CHEMTECH* **21,** 304–309
44. Szajnman, S. H., Bailey, B. N., Docampo, R., and Rodriguez, J. B. (2001) *Bioorg. Med. Chem. Lett.* **11,** 789–792
45. Eubank, W. B., and Reeves, R. E. (1982) *J. Parasitol.* **68,** 599–602
46. Shinoda, H., Adamek, G., Felix, R., Fleisch, H., Schenk, R., and Hagan, P. (1983) *Calcif. Tissue Int.* **35,** 87–99
47. van Beek, E., Pieterman, E., Cohen, L., Löwik, C., and Papapoulos, S. (1999) *Biochem. Biophys. Res. Commun.* **255,** 491–494
48. Widler, L., Jaeggi, K. A., Glatt, M., Muller, K., Bachmann, R., Bisping, M., Born, A. R., Cortesi, R., Guiglia, G., Jeker, H., Klein, R., Ramseier, U., Schmid, J., Schreiber, G., Seltenmeyer, Y., and Green, J. R. (2002) *J. Med. Chem.* **45,** 3721–3738
49. Sicard, H., Al Saati, T., Delsol, G., and Fournié, J. J. (2001) *Mol. Med.* **7,** 711–722
50. Reilly, J. F., Martinez, S. D., Mickey, G., and Maher, P. A. (2002) *Biochem. J.* **366,** 501–510
51. Wang, L., Kamath, A., Das, H., Li, L., and Bukowski, J. F. (2001) *J. Clin. Invest.* **108,** 1349–1357
52. Das, H., Wang, L., Kamath, A., and Bukowski, J. F. (2001) *Blood* **98,** 1616–1618